# We are IntechOpen, the world's leading publisher of Open Access books Built by scientists, for scientists

**4,800**
Open access books available

**122,000**
International authors and editors

**135M**
Downloads

Our authors are among the

**154**
Countries delivered to

**TOP 1%**
most cited scientists

**12.2%**
Contributors from top 500 universities

CLARIVATE ANALYTICS BOOK CITATION INDEX INDEXED

WEB OF SCIENCE™

Selection of our books indexed in the Book Citation Index in Web of Science™ Core Collection (BKCI)

## Interested in publishing with us?
## Contact book.department@intechopen.com

Numbers displayed above are based on latest data collected.
For more information visit www.intechopen.com

Chapter

# A Novel Class of Super-Elliptical Vivaldi Antennas for Ultra-Wideband Applications

*Abraham Loutridis, Simay Kazıcı, Oleg V. Stukach, Arman B. Mirmanov and Diego Caratelli*

## Abstract

A novel class of complex-shaped antipodal Vivaldi antennas with enhanced impedance matching characteristics and an equivalent fractional bandwidth (FBW) of 166.8% is proposed. The reported antenna geometry is designed using the super-ellipse equation and implemented using an inexpensive FR4 laminate having a size of 170.7 mm × 134 mm × 0.2 mm. The presented low-cost, easy-to-fabricate radiating structure yields typical total efficiency, realized gain, and front-to-back ratio of 68%, 8.2 dBi, and 21.1 dB, respectively, across the operational frequency range. A parameter study of key geometrical features of the antenna is detailed in order to provide useful design guidelines while getting a better insight into the relevant physical behavior. Finally, a prototype is realized and characterized. The numerical results collected by full-wave simulation of the antenna structure are found to be in good agreement with the experimental measurements taken on the physical demonstrator.

**Keywords:** antipodal Vivaldi antennas, ultra-wideband, super-ellipse formula

## 1. Introduction

High data rates (up to 50 Mbps within a range of 10 m), low power consumption, and minimal interference make ultra-wideband (UWB) technology an attractive solution for short-range wireless communication [1]. Although the spectrum allocated for UWB technology overlaps existing frequency bands, the very low power levels (regulated by the Federal Communications Commission) prevent interference.

Among various broadband radiating structures such as printed dipoles [2], monopoles [3], bow-ties [4–6], patch antennas [7–8], dielectric resonator, and lens antennas [9–11], tapered slot antennas (TSAs) exhibit the most favorable performance in terms of bandwidth and radiation pattern characteristics. For example, Vivaldi antennas, a special subclass of TSAs, offer large bandwidth and flat gain over the frequency range; in addition, they present compact and robust system integration properties in a wide range of fields, including wireless communication, microwave imaging, millimeter-wave applications, ground penetrating radar, remote sensing [12], and biomedical screening and diagnosis [13–18].

Vivaldi antennas were first proposed by Gibson in 1979 [19]. Subsequently, Gazit developed antipodal Vivaldi antennas (AVAs) comprising two metallic plates placed on the top and bottom sides of a low-permittivity substrate, forming an antipodal slotline transition [20]. This antenna configuration is characterized by a simpler feeding mechanism and delivers a wider operational bandwidth than Gibson's proposal.

Several AVA configurations have since been proposed in the literature [21–25]. These solutions have improved the radio-frequency (RF) characteristics of the antennas, but they have also unduly complicated the antenna geometry, thus increasing the manufacturing costs and even performance deviations due to tolerances and inaccuracies during fabrication.

As is well known from theory, the tapering of the aperture strongly influences the antenna radiation characteristics [26–29]. In this paper, a new type of AVA is proposed, namely the super-elliptical antipodal Vivaldi antenna (SAVA). Compared with conventional AVAs, the SAVA has more favorable RF characteristics, such as extended bandwidth, larger front-to-back ratio (FBR), and higher gain flatness. Herein, the proposed antenna is designed, and its circuital characteristics and radiation properties optimized for the 1.14–12.6 GHz frequency band.

## 2. Antenna design and simulation

### 2.1 Factors influencing antenna performance

The radiation mechanism of a Vivaldi antenna (**Figure 1**) is such that it works as a resonator at low frequencies and as a traveling-wave radiator at high frequencies. The lower cut-off frequency depends strongly on the width of the antenna (i.e., the maximum separation between the two arms), whereas the lower cut-off wavelength is around $\lambda/2$ for a given low-frequency band.

The thickness of the substrate strongly influences antenna performance. As the thickness increases, undesired modes become increasingly excited. These modes change the phase of the traveling waves along the two flares to create pattern distortion, resulting in high cross-polarization. Therefore, thin substrates composed of low-dielectric materials are preferred. Furthermore, the electrical length of the radiating antipodal flares determines the phase difference of the traveling-wave currents. Hence, this factor affects the broadband performance of the antenna and determines the higher and lower cut-off frequencies as well as antenna gain [26–29].

### 2.2 Antenna design and fabrication

The proposed Vivaldi antenna was modeled using CST Microwave Studio (version 2019) as follows. The antenna was printed on a thin 171 mm ($0.6\lambda_0$ at 1.14 GHz) $\times$ 134 mm ($0.5\lambda_0$ at 1.14 GHz) FR4 substrate ($\epsilon_r$ = 4.15, tan$\delta$ = 0.02, thickness = 0.2 mm) with a double-sided copper metallization thickness of 0.035 mm. The antenna is fed by a 50-Ω 0.36-mm-long microstrip on the front side of the substrate and connected directly to a 50-Ω SMA connector. A metallic thin radiator, placed on the front side of the PCB layer, is connected to the microstrip line using a highly smooth transition. The antipodal metallic radiator and the grounding plane of the microstrip feeding line are placed on the rear side of the PCB layer.

### 2.3 Super-ellipse formula in antenna design

In 1818, the French mathematician Gabriel Lamé introduced the following super-ellipse formula:

$$\left|\frac{x}{a}\right|^m + \left|\frac{y}{b}\right|^n = 1 \tag{1}$$

In Eq. (1), $a$ and $b$ denote the semi-axes of the super-ellipse, whereas the positive real-valued parameters $m$ and $n$ control the convexity of the curve. In this study, to improve RF characteristics, we use Eq. (1) to describe the radiating flares and feeding structure of the antenna (**Figure 1**). The resulting antennas are referred to as super-elliptical antipodal Vivaldi antennas (SAVAs). A parametric version of Eq. (1) is given hereafter:

$$\begin{cases} x(t) = a|\cos t|^m \\ y(t) = b|\sin t|^n \end{cases} \tag{2}$$

The default values of $m$ and $n$ are set to 2. Analytical curves are created on the basis of Eq. (2) and implemented in the antenna model built in CST Microwave Studio. The super-elliptical analytical curves shape the antenna contour to the special geometry shown in **Figure 1**. The radiating structure in **Figure 1** consists of quarter-ellipses with major semi-axes b1, a2, a3, and a3_1 and minor semi-axes a1, b2, and b3.

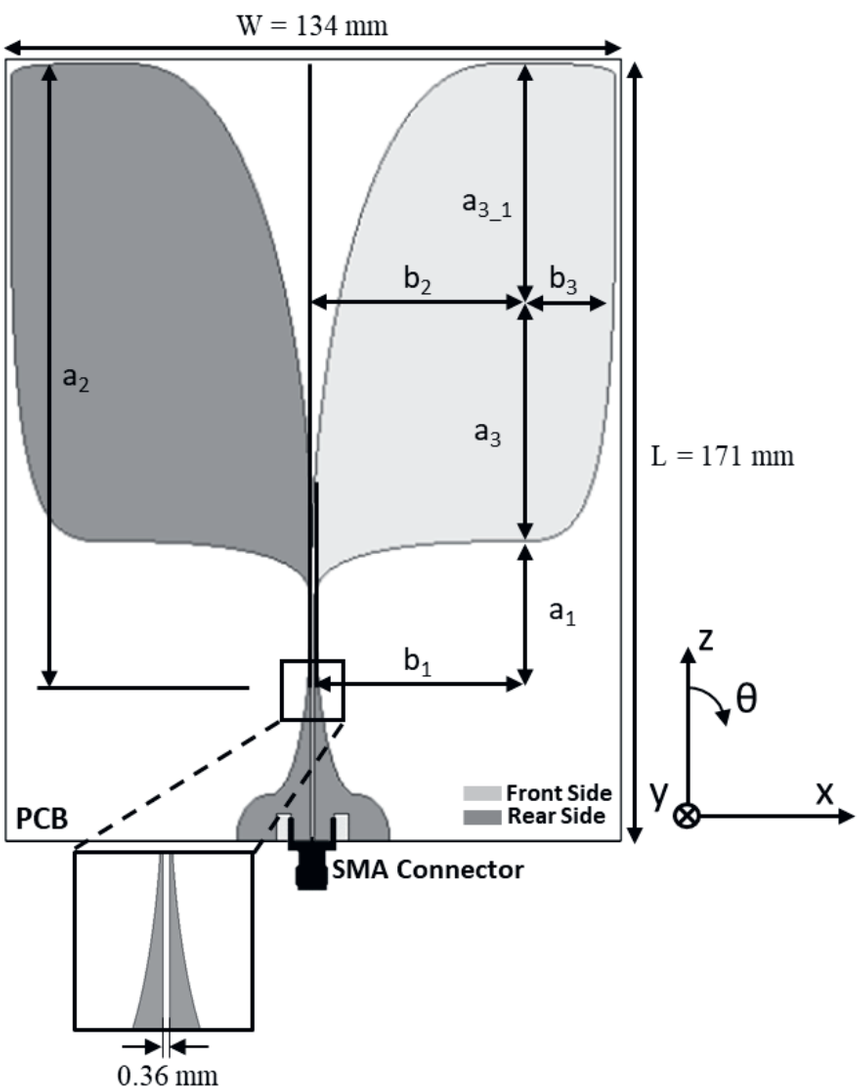


**Figure 1.**
*Antenna geometry of a Vivaldi antenna and its coordinate system.*

Similarly, the antenna feeding structure is designed using Eq. (1). Both the ground plane and the feeding microstrip line consist of quarter-ellipses. Note that the various sections of the antenna in **Figure 2** are characterized by different ellipticity parameters *m* and *n*, depending on the parametric representation (2).

### 2.4 Parametric investigation

This section discusses the parametric investigation of the variation of the voltage standing wave ratio (VSWR) with respect to six key parameters—namely n1, n2, n3, m1, m2, and m3—of the SAVA antenna shown in **Figure 2**. In the parametric simulations that follow, all parameters apart from the parameter of interest were set to 2.

**Figure 3** shows the effect of parameter n1, which was varied from 0.5 to 3. The simulated results show that the impedance-matching properties of the antenna are strongly dependent on n1, with strong variations evident in the 3–12 GHz frequency

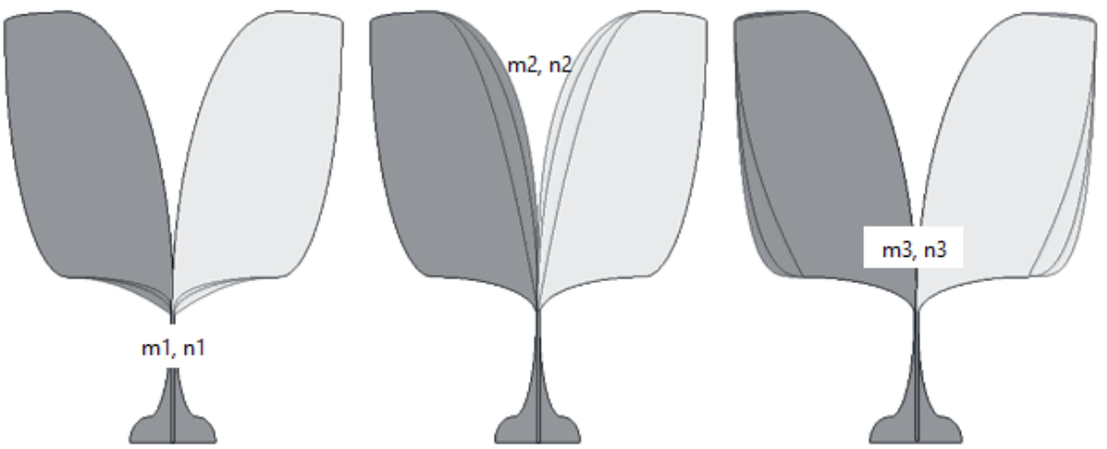


**Figure 2.**
*Application of super-ellipse formula to antenna geometry.*

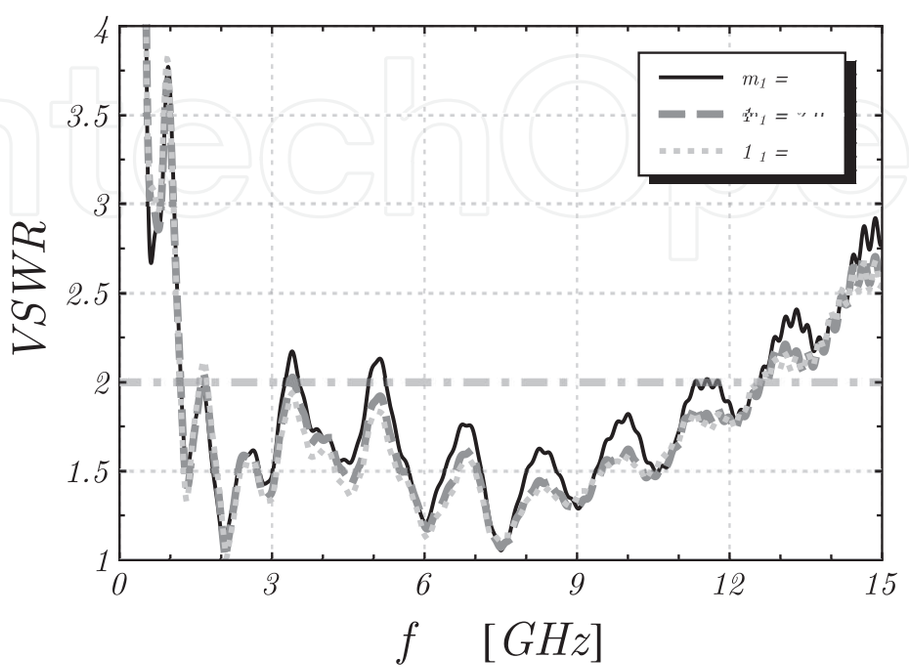


**Figure 3.**
*Simulated VSWR dependence on n1.*

range. The optimal value of n1 was identified to be 3, with this enabling a VSWR smaller than 2:1 over across a frequency range of nearly three octaves (an octave is a doubling of frequency).

**Figure 4** depicts the simulated VSWR dependence on parameter m1, which was varied from 0.5 to 4. One can notice that the impedance-matching characteristics of the antenna tend to improve, especially in the upper band of the operational frequency range, as m1 becomes larger. Optimal performance is achieved for m1 = 2.

Similarly, **Figures 5** and **6** show the effect of n2 and m2 on VSWR, which were varied from 1 to 3 and from 0.5 to 2, respectively. From the simulated data, it is

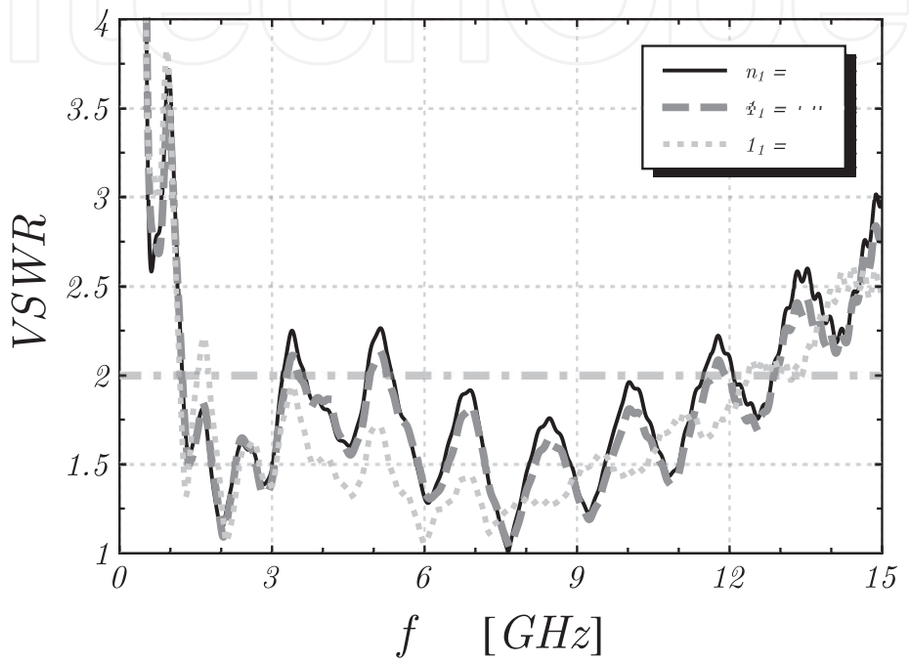


**Figure 4.**
*Simulated VSWR dependence on m1.*

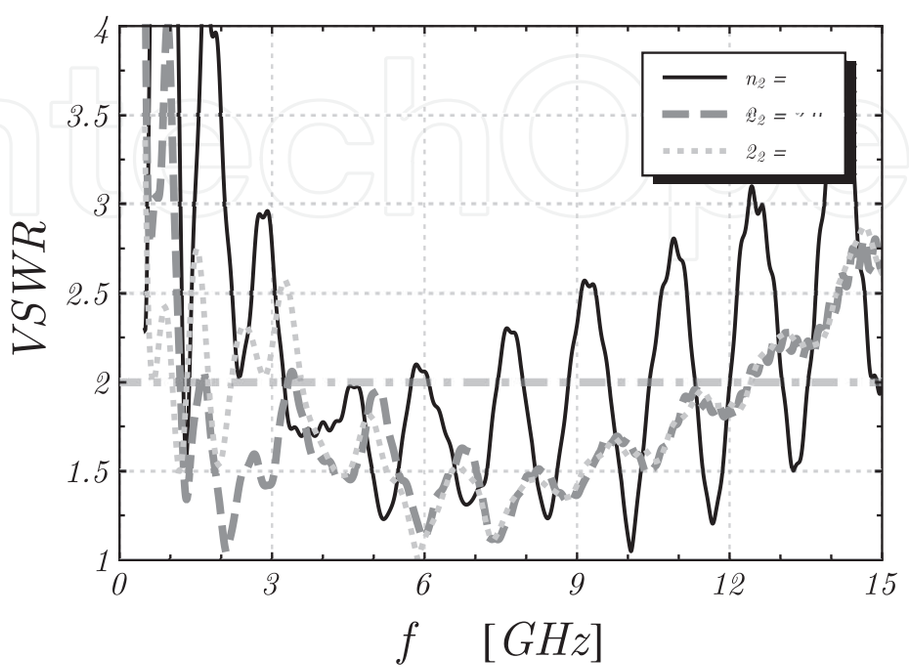


**Figure 5.**
*Simulated VSWR dependence on n2.*

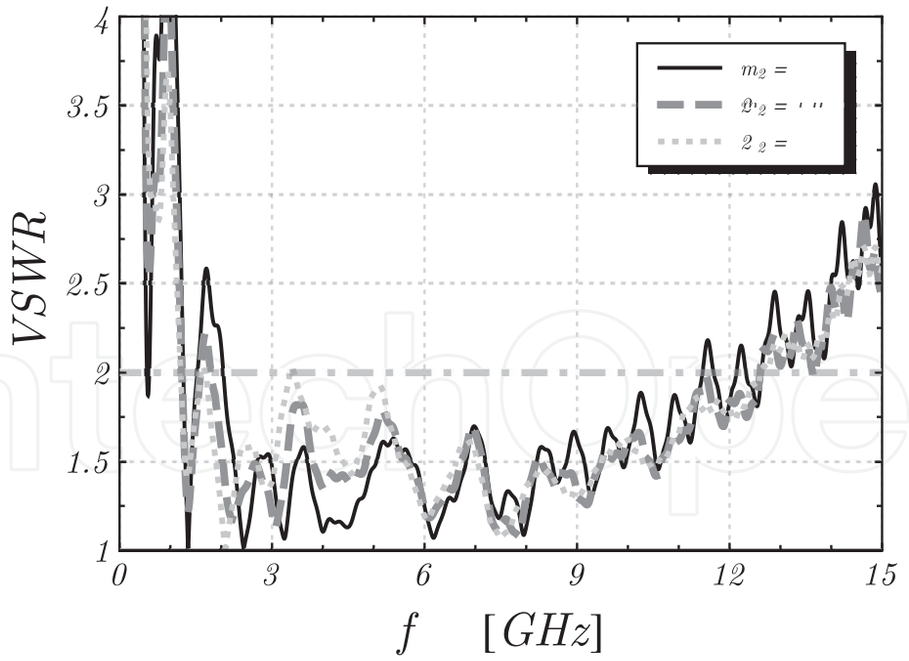


**Figure 6.**
*Simulated VSWR dependence on m2.*

apparent that improved performance in terms of reduced VSWR is achieved, wherein both n2 and m2 are selected to be 2.

**Figures 7** and **8** similarly illustrate the effect of n3 and m3, which were varied from 0.5 to 3 and from 0.5 to 4, respectively. The simulations clarify that the VSWR antenna response does not depend heavily on either n3 or m3. The optimal values of n3 and m3 were identified to be 3 and 4, respectively.

Finally, to optimize the shape of the two antenna flares, the aforementioned optimized values of n1, n2, n3, m1, m2, and m3 were used as inputs in a particle swarm optimization (PSO) procedure.

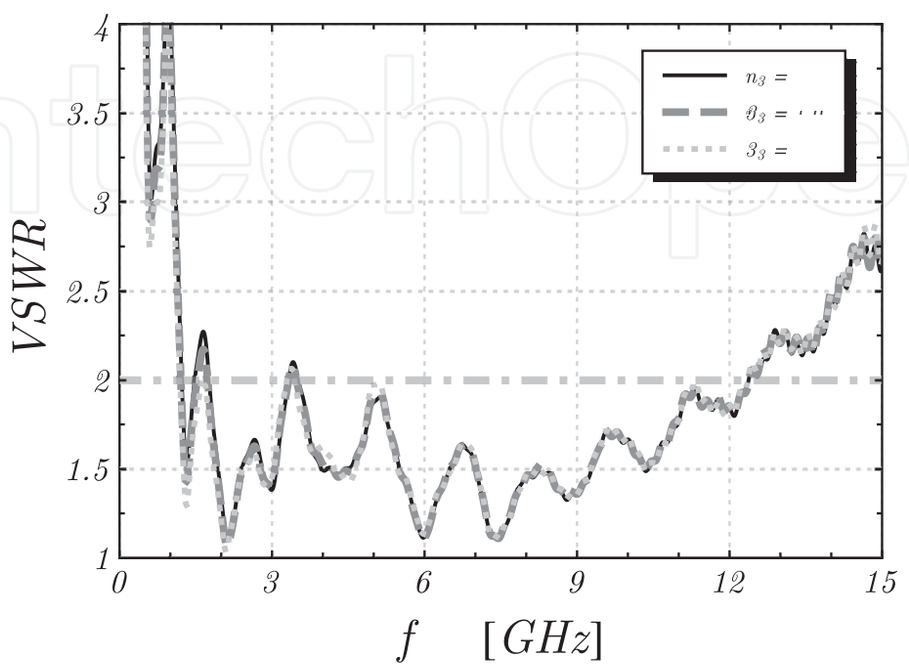


**Figure 7.**
*Simulated VSWR dependence on n3.*

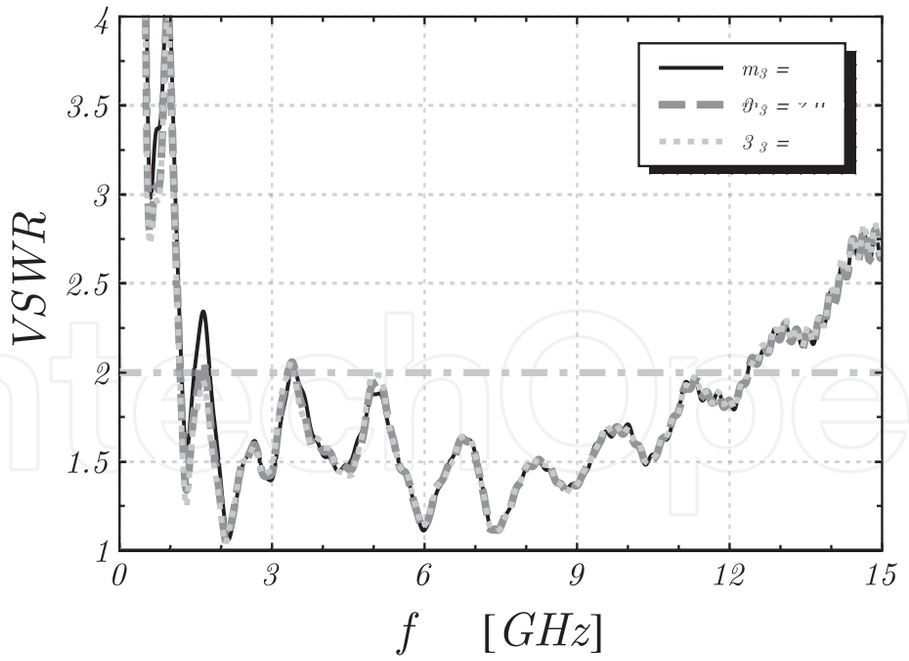


**Figure 8.**
*Simulated VSWR dependence on m3.*

With the end goal of improving antenna performance, the two main objectives of the PSO procedure were as follows:

1. achieve broader bandwidth (BW) $[f_H - f_L]$ in absolute terms ($f_H$ = higher cut-off frequency at a 2:1 VSWR level, $f_L$ = lower cut-off frequency at a 2:1 VSWR level) and

2. decrease the lower cut-off frequency $f_L$.

The PSO-optimized values for the six parameters were as follows: n1 = 3.15, m1 = 2.25, n2 = 2.05, m2 = 2.35, n3 = 3.451, and m3 = 4.3.

## 3. Antenna prototype characterization

The SAVA optimized in Section II was prototyped and characterized comparatively against conventional antipodal Vivaldi antenna (CAVA) configurations.

### 3.1 VSWR, efficiency, realized gain, and FBR

**Figure 9** presents a comparison of the VSWR performance of the SAVA and CAVA configurations. Clearly, the SAVA features substantially more favorable impedance-matching properties and a lower cut-off frequency, without compromising on compactness. The SAVA had a measured impedance bandwidth (for VSWR < 2:1) of 11.46 GHz (1.14–12.6 GHz) with a fractional bandwidth of 166.8%. Please note that the reported performance figures are in excellent agreement (within 5% difference) with the numerical results obtained by full-wave simulation of the radiating structure. By contrast, the CAVA had a significantly smaller bandwidth of 9.46 GHz (1.21–10.67 GHz), with a fractional bandwidth of 159.2%.

The radiation properties of both the antenna configurations were characterized using a near-field scanner (MVG StarLab) in the 0.6–18 GHz frequency range. The

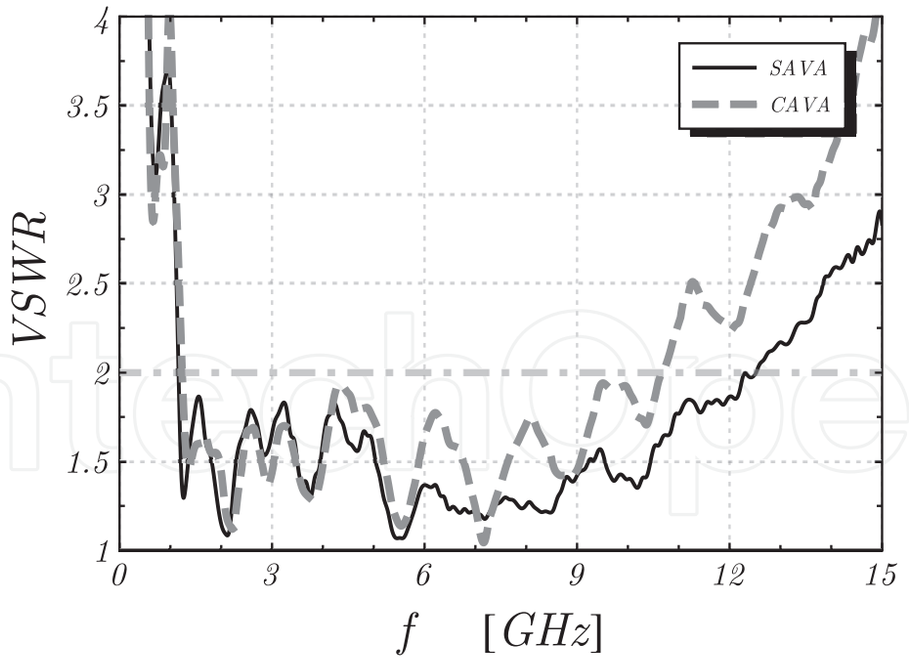


**Figure 9.**
*Measured VSWR performance of the SAVA and CAVA antennas.*

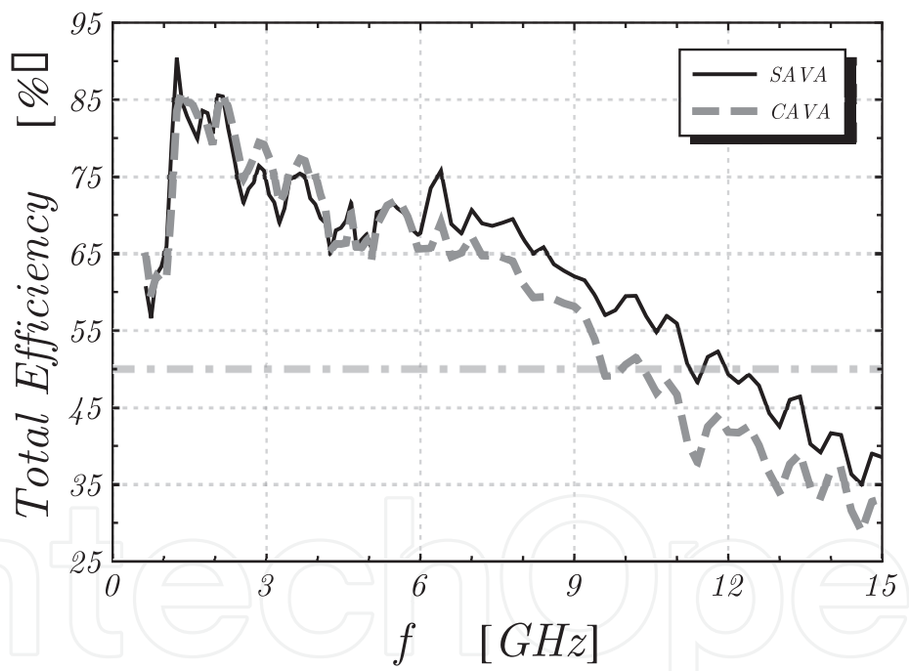


**Figure 10.**
*Measured total efficiency of the SAVA and CAVA antennas.*

average efficiency, realized gain, and FBR across the operational frequency band were 68.5%, 8.2 dBi, and 21.1 dB, respectively, for the SAVA, whereas the corresponding values were 62%, 7.9 dBi, and 19.5 dB, respectively, for the CAVA (**Figures 10–12**).

**Figures 13** and **14** show the measured radiation patterns of the SAVA along two elevation planes ($\phi$ = 0° and 90°) at working frequencies of 2, 6, and 10 GHz. At low frequencies, the proposed antenna exhibits good directional radiation patterns, with smooth contours in both elevation planes. As the operating frequency increases, strong ripples appear in the peripheries of the radiation patterns due to the excitation of higher-order modes.

The SAVA antenna has end-fire characteristic with the main lobe in the axial direction (here, in z-direction) of the tapered slot.

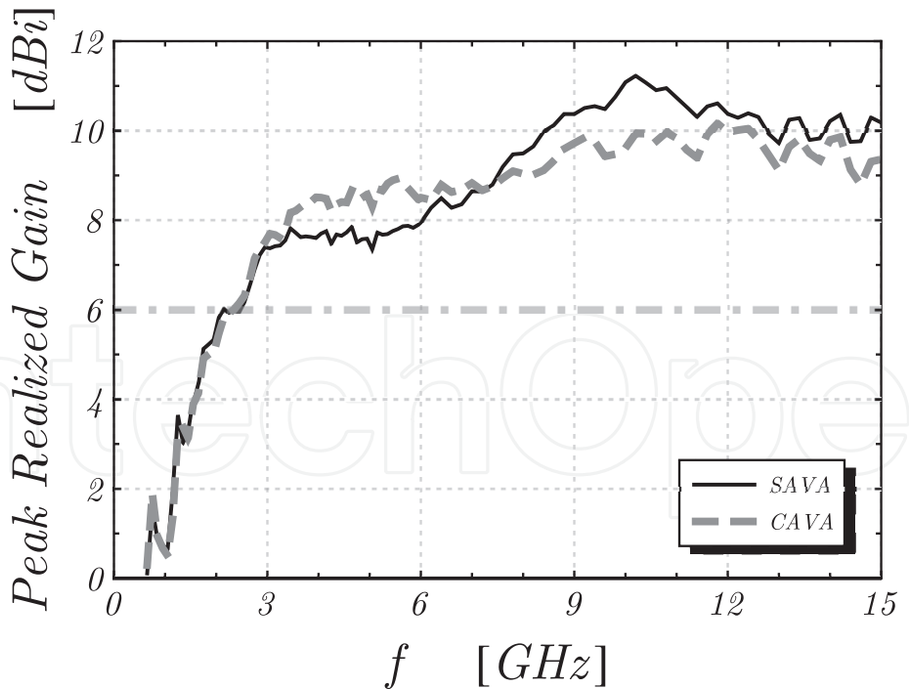


**Figure 11.**
*Measured peak realized gain of the SAVA and CAVA antennas.*

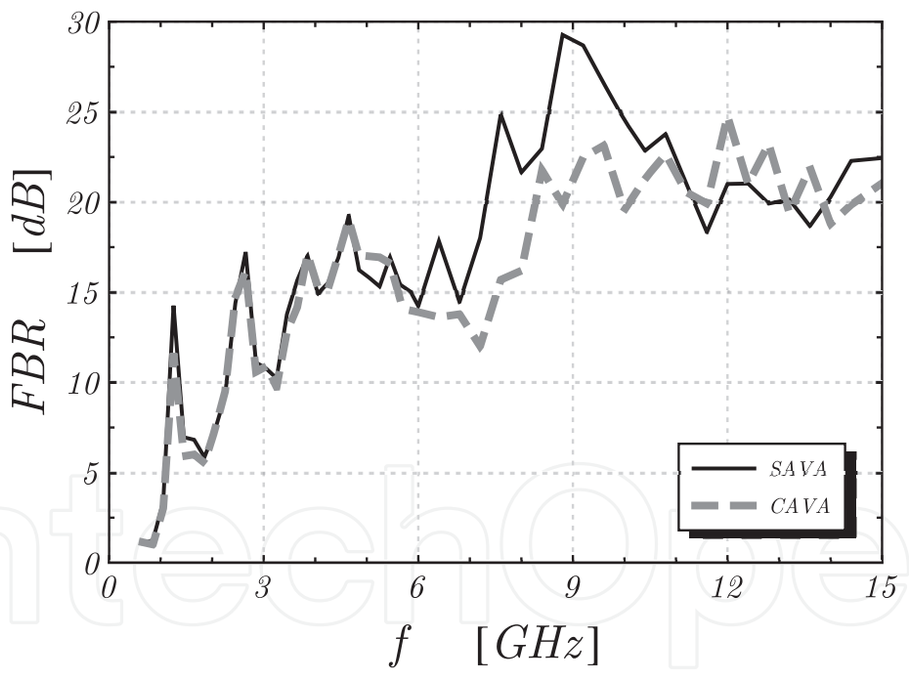


**Figure 12.**
*Measured FBR of the SAVA and CAVA antennas.*

### 3.2 Fidelity factor

The fidelity factor [30–31] quantifies the degree to which a radiated electric field (E-field) waveform of a transmitting antenna resembles the input pulse. As the amplitude of the E-field waveform is expected to differ from that of the input pulse, the E-field waveform and the input pulse are normalized to compare only the shape:

$$\hat{i}(t) = \frac{i(t)}{\left[\int_{-\infty}^{+\infty} |i(t)|^2 dt\right]^{\frac{1}{2}}} \tag{3}$$

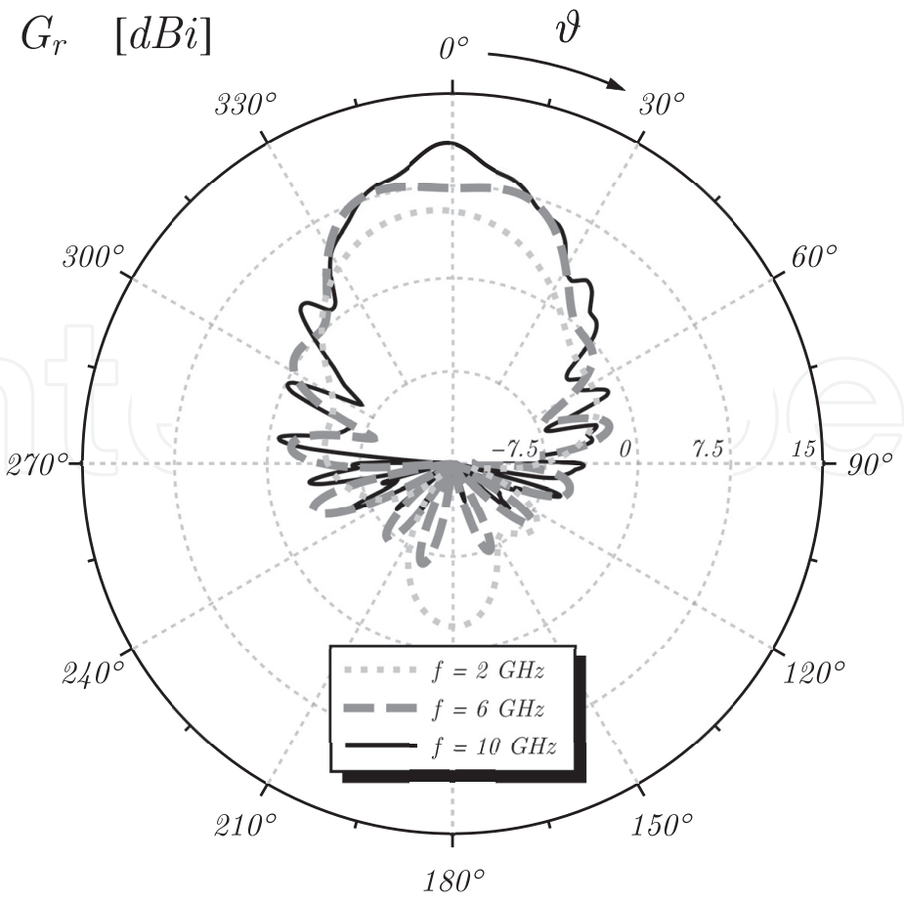


**Figure 13.**
*Measured radiation patterns of the SAVA antenna along the cut plane $\phi = 0°$ at the working frequency of 2, 6, and 10 GHz.*

$$\hat{e}(t) = \frac{e(t)}{\left[\int_{-\infty}^{+\infty} |e(t)|^2 dt\right]^{\frac{1}{2}}} \tag{4}$$

The degree of correlation between Eqs. (3) and (4) is quantified as the fidelity factor:

$$\begin{aligned} FF &= \max_{\tau} \int_{-\infty}^{+\infty} \hat{i}(t)\hat{e}(t-\tau)dt \\ &= \max_{\tau} \left\{ \frac{\int i(t)e(t-\tau)dt}{\sqrt{\int i^2(t)dt}\sqrt{\int e^2(t)dt}} \right\} \end{aligned} \tag{5}$$

The fidelity factor varies from 0 to 1, with 1 indicating that the E-field waveform is identical to the input pulse and that no distortion occurs during transmission.

To calculate the fidelity factor in this work, a Gaussian-modulated pulse in the desired frequency band (3.1–10.6 GHz) was used as the input signal, with ideal filed probes placed at the far field of the transmitting antenna. **Figure 15** illustrates the fidelity factor distribution along the H-plane of the SAVA and CAVA antennas. Clearly, the proposed SAVA configuration outperforms the CAVA configuration in both planes.

### 3.3 Group delay

Group delay, defined as the derivative of phase response ($\angle H(\omega)$) versus frequency [32], is used to characterize two port system (e.g., filters, amplifiers, and mixers).

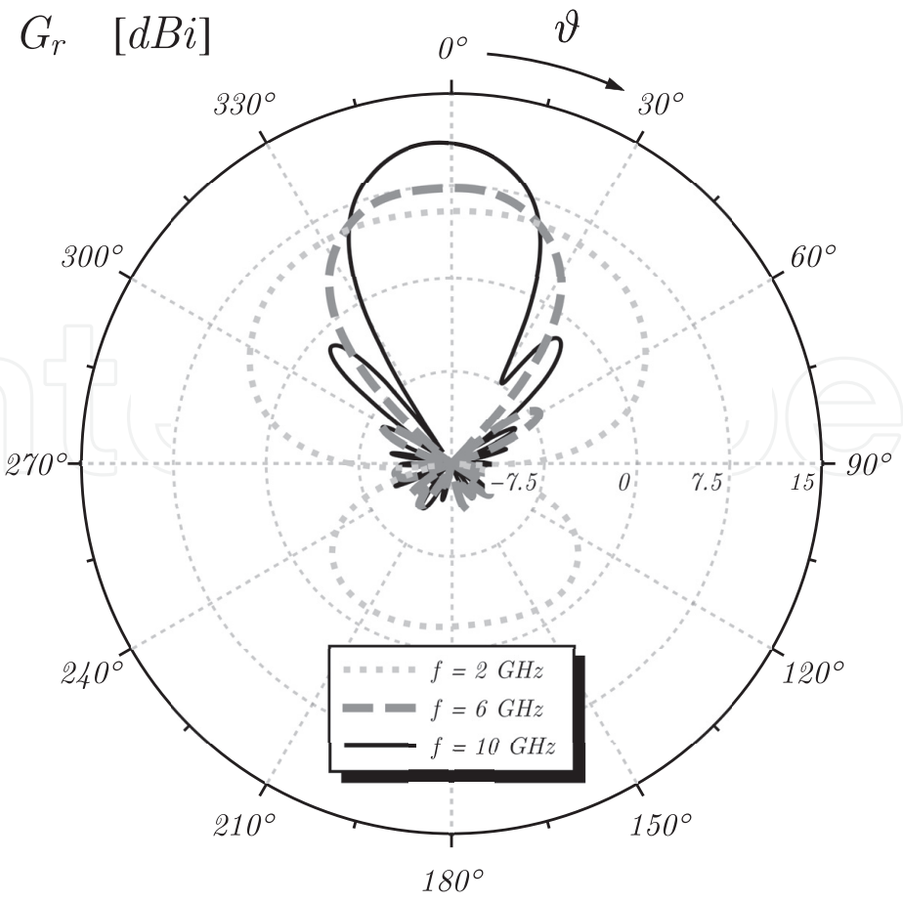


**Figure 14.**
*Measured radiation patterns of the SAVA antenna along the cut plane $\phi = 90°$ at the working frequency of 2, 6, and 10 GHz.*

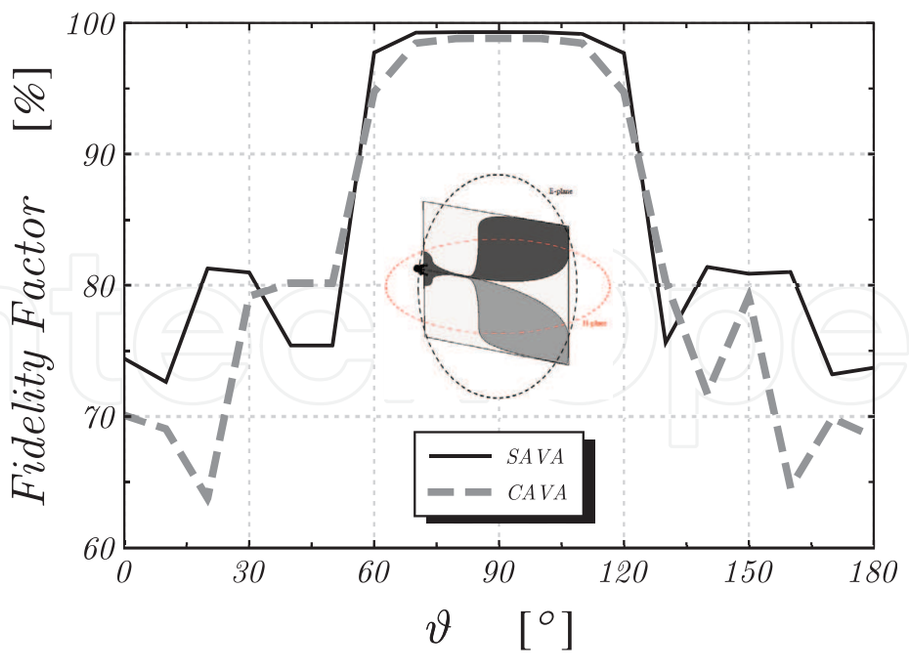


**Figure 15.**
*Fidelity factor characteristics of the SAVA and CAVA antennas along the H-plane.*

$$\tau = -\frac{d[\angle H(\omega)]}{d\omega} = -\frac{1}{360^{\circ}}\frac{d[\angle H(f)]}{df} \tag{6}$$

This factor has previously been applied to UWB antenna systems [32]. It measures the total phase distortion of the antenna system, using which the dispersion of

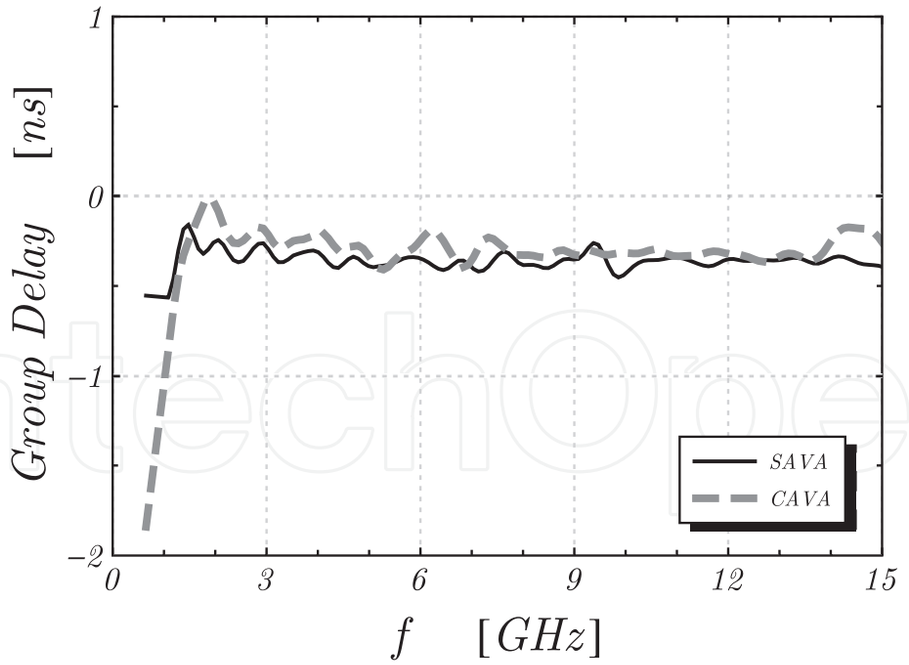


**Figure 16.**
*Measured group delay of the SAVA and CAVA antennas.*

the transmitted signal can be inferred. For a given frequency, the average group delay represents the time required for a signal to travel from one antenna terminal to the other.

The group delay of both the SAVA and CAVA configurations was measured in a free space environment. A network analyzer was used to measure the S21 group delay between two identical antennas (in each configuration) placed 2.5 m apart (i.e., far-field conditions) and aligned with the E-plane (**Figure 16**).

Clearly, the SAVA shows a smoother and more linear behavior, whereas the CAVA exhibits strong group delay variation, indicating phase nonlinearity along most of the frequency band.

## 4. Conclusion

This work has proposed a novel class of SAVAs. The geometry of the considered radiating structures is optimized by means of the super-ellipse formula, thus achieving UWB operation. Compared with current conventional Vivaldi antenna configurations, the proposed topology yields compelling benefits in terms of better impedance-matching properties, larger efficiency, gain, and front-to-back radiation ratio across a broad frequency range, without compromising on antenna compactness. The high directional radiation characteristics of SAVAs make them suitable for several applications, such as UWB communications and remote sensing, microwave imaging, ground penetrating radar, and biomedical screening.

*DOI: http://dx.doi.org/10.5772/intechopen.92325*



## Author details

Abraham Loutridis[1], Simay Kazıcı[2], Oleg V. Stukach[3], Arman B. Mirmanov[4] and Diego Caratelli[2,5*]

1 Alps Alpine Europe, Munich, Germany

2 The Antenna Company, Eindhoven, The Netherlands

3 Higher School of Economics (HSE), National Research University, Moscow, Russia

4 Seifullin Kazakh Agro Technical University, Astana, Kazakhstan

5 Eindhoven University of Technology, Eindhoven, The Netherlands

*Address all correspondence to: diego.caratelli@antennacompany.com

## References

[1] Foerster J, Green E, Somayazulu S, Leeper D. Ultra-wideband technology for short-or medium-range wireless communications. Intel Technology Journal. 2001;**5**(2):1-11

[2] Paraforou V, Tran D, Caratelli D. A novel supershaped slot-loaded printed dipole antenna with broadside radiation for dual-band WLAN applications. In: Proceedings of the European Conference on Antennas and Propagation; The Hague, The Netherlands; 6–11 April 2014. pp. 3460-3463

[3] Caratelli D, Mescia L, Bia P. Design and full-wave characterization of supershaped printed monopole antennas. In: Proceedings of the IEEE AP-S/URSI Symposium; San Diego, California, U.S.A.; 9–14 July 2017. pp. 1769-1770

[4] Caratelli D, Yarovoy A, Ligthart LP. Full-wave analysis of cavity-backed resistively-loaded bow-tie antennas for GPR applications. In: Proceedings of European Radar Conference; 2008. pp. 204-207

[5] Caratelli D, Yarovoy A. Design and full-wave analysis of cavity-backed resistively loaded circular-end bow-tie antennas for GPR applications – Part I. Applied Computational Electromagnetics Society Journal. 2010; **25**:809-817

[6] Caratelli D, Yarovoy A. Design and full-wave analysis of cavity-backed resistively loaded circular-end bow-tie antennas for GPR applications – Part II. Applied Computational Electromagnetics Society Journal. 2010;**25**:818-829

[7] Paraforou V, Tran D, Caratelli D. A dual-band supershaped annular slotted patch antenna for WLAN systems. In: Proceedings of European Conference on Antennas and Propagation; The Hague, The Netherlands; 6–11 April 2014. pp. 2762-2764

[8] Samaras KA, Maximidis RT, Koutinos A, Caratelli D, Sahalos JN, Kyriacou GA. Characteristic mode analysis of drop-like supershaped patch antenna. In: Proceedings of International Conference on Modern Circuits and Systems Technologies; Thessaloniki, Greece; 7–9 May 2018

[9] Simeoni M, Cicchetti R, Yarovoy A, Caratelli D. Plastic-based supershaped dielectric resonator antennas for wide-band applications. IEEE Transactions on Antennas and Propagation. 2011;**59**(12): 4820-4825

[10] Bia P, Caratelli D, Mescia L, Gielis J. Analysis and synthesis of supershaped dielectric lens antennas. In: IET Microwaves, Antennas and Propagation. IET. 2015;**9**:1497-1504. DOI: 10.1049/iet-map.2015.0091

[11] Mescia L, Bia P, Caratelli D, Chiapperino MA, Stukach O, Gielis J. Electromagnetic mathematical modeling of 3D supershaped dielectric lens antennas. Hindawi Mathematical Problems in Engineering. 2016;**2016**: 8130160, 1-8130110. DOI: 10.1155/2016/8130160

[12] Lay-Ekuakille A, Vergallo P, Giannoccaro NI, Massaro A, Caratelli D. Prediction and validation of outcomes from air monitoring sensors and networks of sensors (Invited). In: Proceedings of 5th International Conference on Sensing Technology; Palmerston North, New Zealand; 28 November-1 December 2011. pp. 78-83

[13] Biswas B, Ghatak R, Poddar D. A fern fractal leaf inspired wideband antipodal Vivaldi antenna for microwave imaging system. IEEE Transactions on Antennas and Propagation. 2017;**65**(11):6126-6129

[14] Zhu S, Liu H, Chen Z, Wen P. A compact gain-enhanced Vivaldi antenna array with suppressed mutual coupling for 5G mmWave application. IEEE Antennas and Wireless Propagation Letters. 2018;**17**(5):776-779

[15] Baldi M, Cerri G, Chiaraluce F, Eusebi L, Russo P. Non-invasive UWB sensing of astronauts' breathing activity. Sensors. 2015;**15**(1):565-591

[16] Pumallica-Paro MA, Arizaca-Cusicuna JL, Clemente-Arenas M. Optimizing cutoff frequency in an antipodal Vivaldi antenna for GPR applications through a novel balun. In: IEEE XXV International Conference on Electronics, Electrical Engineering and Computing (INTERCON). IEEE; 2018

[17] Alzabidi MA, Aldhaeebi MA, Elshafiey I. Optimization of UWB Vivaldi antenna for tumor detection. In: 1st International Conference on Artificial Intelligence, Modelling and Simulation; IEEE; 2013

[18] Yang K, Loutridis A, Bao X, McEvoy P, Ammann MJ. A coplanar Vivaldi antenna with integrated filter for Ka-band. In: Loughborough Antennas & Propagation Conference (LAPC); UK; 1–4 November 2016

[19] Gibson P. The Vivaldi aerial. In: 9th European Microwave Conference; IEEE; 1979

[20] Gazit E. Improved design of the Vivaldi antenna. In: IEEE Proceedings H (Microwaves, Antennas and Propagation); IET; 1988

[21] Puskely J, Lacik J, Raida Z, Arthaber H. High-gain dielectric-loaded Vivaldi antenna for Ka-band applications. IEEE Antennas and Wireless Propagation Letters. 2016;**15**: 2004-2007

[22] Wang H, He S, Ding Z, Cao J, Yang Y. A miniaturized Vivaldi antenna with high gain for ultra-wideband applications. In: Sixth Asia-Pacific Conference on Antennas and Propagation; IEEE; 2017

[23] Belen MA, Evranos İO, Güneş F. Gain enhancement of antipodal Vivaldi antenna, In: 26th Signal Processing and Communications Applications Conference (SIU); IEEE; 2-5 May 2018

[24] Herzi R, Bouslama M, Osman L, Gharsallah A. Design of a compact antipodal Vivaldi antenna with band-rejected characteristic. In: Mediterranean Microwave Symposium (MMS); IEEE; 28-30 Nov. 2017

[25] Fernandez-Martinez P, Martin-Anton S, Segovia-Vargas D. Design of a wideband Vivaldi antenna for 5G base stations. In: IEEE International Symposium on Antennas and Propagation and USNC-URSI Radio Science Meeting; IEEE; 7-12 July 2019

[26] Nassar IT, Weller TM. A novel method for improving antipodal vivaldi antenna performance. IEEE Transactions on Antennas and Propagation. 2015;**63**(7):3321-3324

[27] De Oliveira AM, Perotoni MB, Kofuji ST, Justo JF. A palm tree antipodal Vivaldi antenna with exponential slot edge for improved radiation pattern. IEEE Antennas and Wireless Propagation Letters. 2015;**14**: 1334-1337

[28] Amiri M, Tofigh F, Ghafoorzadeh-Yazdi A, Abolhasan M. Exponential antipodal Vivaldi antenna with exponential dielectric lens. IEEE Antennas and Wireless Propagation Letters. 2017;**16**:1792-1795

[29] Karmakar A, Saha A, Bhattacharjee A, Bhawal A. In: Design of a fractal based wideband antipodal Vivaldi antenna with improved radiation characteristics for biomedical applications. In: Fourth International

Conference on Research in Computational Intelligence and Communication Networks (ICRCICN); IEEE; 22-23 Nov. 2018

[30] Kwon D-H. Effect of antenna gain and group delay variations on pulse-preserving capabilities of ultrawideband antennas. IEEE Transactions on Antennas and Propagation. 2006;**54**(8): 2208-2215

[31] Liu J, Eisele KP, Hay SG, Zhong S. Effects of printed UWB antenna miniaturization on pulse fidelity and pattern stability. IEEE Transactions on Antennas and Propagation. 2014;**62**(8): 3903-3910

[32] Zhu X, Li Y, Yong S, Zhuang Z. A novel definition and measurement method of group delay and its application. IEEE Transactions on Instrumentation and Measurement. 2009;**58**(1):229-233